Centrifugal quantum states of neutrons

V. V. Nesvizhevsky* and A. K. Petukhov
Institut Laue-Langevin (ILL), 6 rue Jules Horowitz, F-38042, Grenoble, France

K. V. Protasov
Laboratoire de Physique Subatomique et de Cosmologie (LPSC), IN2P3-CNRS, UJFG, 53, Avenue des Martyrs, F-38026, Grenoble, France

A. Yu. Voronin
P. N. Lebedev Physical Institute, 53 Leninsky prospekt, 119991, Moscow, Russia
(Received 24 June 2008; published 23 September 2008)

We propose a method for observation of the quasistationary states of neutrons localized near a curved mirror surface. The bounding effective well is formed by the centrifugal potential and the mirror Fermi potential. This phenomenon is an example of an exactly solvable "quantum bouncer" problem that can be studied experimentally. It could provide a promising tool for studying fundamental neutron-matter interactions, as well as quantum neutron optics and surface physics effects. We develop a formalism that describes quantitatively the neutron motion near the mirror surface. The effects of mirror roughness are taken into account.

DOI: 10.1103/PhysRevA.78.033616 PACS number(s): 03.75.Be, 03.75.Dg, 03.65.Nk

I. INTRODUCTION

The "centrifugal states" of neutrons is a quantum analog of the so-called whispering gallery wave, the phenomenon which in brief consists of the wave localization near the curved surface of a scatterer. It has been known in acoustics since ancient times and was explained by Rayleigh in his *Theory of Sound* [1,2]. The whispering gallery wave in optics has been an object of growing interest during the last decade [3,4]. In the following we will be interested in the matter-wave aspect of the whispering gallery wave phenomenon: namely, the large-angle neutron scattering on a curved mirror. Such a scattering can be explained in terms of states of a quantum particle above a mirror in a linear potential—the so-called "quantum bouncer" [5–11]. The neutron quantum motion in the Earth's gravitational field above a flat mirror is another example of such a quantum bouncer, which was observed recently [12]. We will show that the centrifugal quantum bouncer and the gravitational quantum bouncer have many common features. Therefore we compare these two phenomena and discuss the motivation for their study.

Experimental observation and study of the gravitational states is a challenging problem which brings rich physical information for searches for extensions of the standard model or for studying the interaction of a quantum system with a gravitational field [13–26], for constraining spin-independent extra short-range forces [27–29], hypothetical axion-mediated spin-matter interactions [30], and in surface physics. Indeed any additional interaction between the mirror bulk and neutron with the characteristic range of the gravitational states of a few micrometers would modify the quantum states and thus could be detected.

A natural extension of the mentioned experimental activity consists in approaching ultimate sensitivity for extra interactions at shorter characteristic ranges. Evidently, the quantum-state characteristic size has to be decreased. To achieve this goal one needs to study novel approaches [31]. We will show that the promising method consists in localization of cold neutrons near a curved mirror surface due to the superposition of the centrifugal potential and the Fermi potential of the mirror. In such a case the quasistationary "centrifugal" quantum states play an essential role in the neutron flux dynamics. In the limit where the centrifugal quantum-state spatial size is much smaller than the curved mirror radius, this problem is reduced to the simple case of a quantum particle in a linear potential above a mirror. Measurement of the gravitationally bound and centrifugal quantum states of neutrons could be considered as a kind of confirmation of the equivalence principle for a quantum particle [32–36]. Both problems (gravitational and centrifugal ones) provide a perfect experimental laboratory for studying neutron quantum optics phenomena, quantum revivals, and localization [37–44]. Evident advantages of using cold neutrons consist in much higher statistics attainable and broad accessibility of cold neutron beams as well as in a crucial reduction of many false effects compared to experiments with gravitationally bound quantum states of neutrons due to approximately $\sim 10^5$ times higher energies of the quantum states involved.

The phenomenon of the centrifugal quantum states of neutrons and the method of their experimental observation are described in Sec. II. In Sec. III we develop the formalism, which describes neutron motion near the curved mirror surface; the properties of the centrifugal quantum states are discussed in Sec. IV. We will show that cold neutrons with a velocity of $\sim 10^3$ m/s are well suited for such experiments. A time-dependent approach is considered in Sec. V. The effects of mirror roughness are taken into account in Sec. VI.

II. PRINCIPLE OF OBSERVATION

If the neutron energy is much larger than the scatterer Fermi potential, most neutrons are scattered in small angles.

*nesvizhevsky@ill.eu

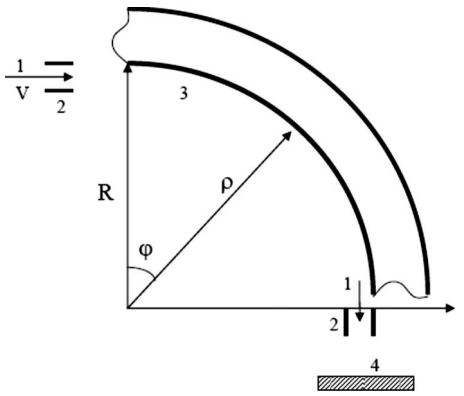

FIG. 1. A scheme of the neutron centrifugal experiment. 1, the classical trajectories of incoming and outcoming neutrons; 2, the collimators; 3, the cylindrical mirror; 4, the detector. Cylindrical coordinates $\rho-\varphi$ used throughout the paper are shown.

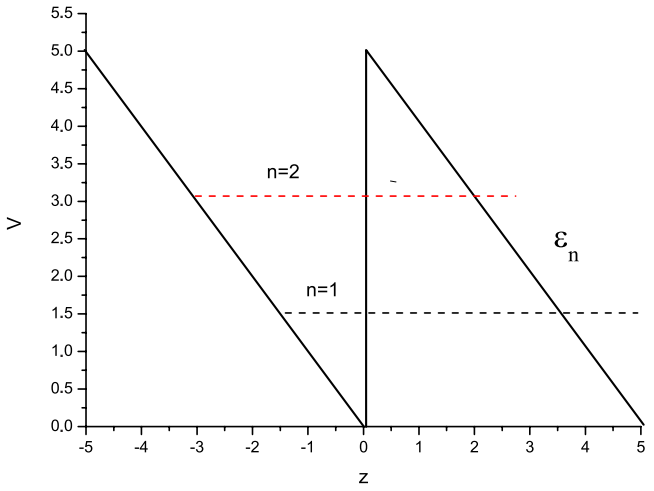

FIG. 2. (Color online) A sketch of the effective potential in the mirror surface vicinity. The potential step at $z=0$ is equal to the mirror Fermi potential in units $\varepsilon_0=[\hbar^2 M v^4/(2R^2)]^{1/3}$. The potential slope at $z\neq 0$ is governed by the centrifugal effective acceleration $a=v^2/R$.

However, some neutrons could be captured into long-living centrifugal quasistationary states localized near the curved scatterer surface and thus could be detected at large deflection angles. The curved mirror surface plays the role of a waveguide, and the centrifugal states play the role of radial modes in such a waveguide. The spectral dependence of the transmission probability is determined by the existence of the centrifugal states in such a system.

Similarly, in the gravitational-state experiment one measures the slit-size dependence of the transmission probability of the waveguide between a mirror and the above-placed absorber [45–54]. The characteristic energy scale of the gravitational-state problem is $\varepsilon_0=0.6$ peV, and the characteristic length scale is $l_0=5.87$ μm. The mirror Fermi potential could be considered as infinitely high and sharp. This approximation is justified as far as l_0 is much larger than the characteristic range of the Fermi-potential increase (typically <1 nm) and ε_0 is much smaller than the characteristic value of the mirror Fermi potential (typically $\sim 10^{-7}$ eV). The methods for experimental observation of the gravitationally bound quantum states of neutrons are based on a relatively large value of the characteristic length l_0, which allowed direct measurement of the shapes of the neutron density distribution in the quantum states using two following complementary methods. The first approach consisted in scanning the neutron density above the mirror using a flat horizontal scatterer/absorber at variable height. The second method is based on use of position-sensitive detectors of UCN with high spatial resolution of ~ 1 μm.

In analogy with the gravitational well the centrifugal quantum well is formed by an effective centrifugal potential and repulsive Fermi potential of a curved mirror as shown in Figs. 1 and 2. The effective acceleration near the curved mirror surface could be approximated as $a=v^2/R$, where v is the neutron velocity and R is the mirror radius. We have significant freedom to choose values of v and R. In particular, it would be advantageous to increase the neutron velocity and to decrease the mirror radius in order to get higher centrifugal acceleration a. In such a case the quantum well that confines the radial motion of neutrons near the curved mirror surface becomes narrower, while the energy of radial motion in the corresponding quantum states increases. This enables us to eliminate many possible systematic effects. The radial motion energy could be as high as the mirror Fermi potential. In this case, we could use the Fermi potential of a mirror as a "filter" for the quantum states. For an ideal cylindrical mirror with perfect shape and zero roughness made of low-absorbing material, neutron losses in such quasistationary quantum states occur via tunneling of neutrons through a triangle potential barrier shown in Fig. 2. The lifetime of deeply bound states is long. The lifetime of the quasistationary quantum states with energy close to the barrier edge is short; such neutrons tunnel rapidly into the mirror bulk. If we vary continuously the centrifugal acceleration (by means of changing the neutron velocity), we will vary the height and the width of the triangle barrier correspondingly and so far the lifetime of the quasistationary quantum states. Due to the very fast (exponential) increase of the mentioned lifetime as a function of the barrier width, we will get a stepwise dependence of the neutron flux parallel to the mirror surface as a function of the neutron velocity. An analogous stepwise dependence of the total neutron flux as a function of the slit size was observed in case of the gravitationally bound quantum states. An alternative method for the observation and study of the centrifugal quantum states consists in measuring the velocity distribution in the quantum states using a position-sensitive neutron detector, placed at some distance from the curved mirror. Such a method was used as well in experimental studies of the gravitationally bound quantum states of neutrons.

It is natural to chose the neutron velocity within the range of maximum intensity of standard neutron sources (neutron reactors or spallation sources) around $\sim 10^3$ m/s. The cylindrical mirror radius has to be equal to a few centimeters in this case, which is just optimal for its production. Neutron beams with high intensity are available in many neutron centers around the world; they could be angularly and spatially collimated; time-of-flight and polarization analyses are avail-

able at standard neutron-scattering instruments. Evidently, the characteristic size of the centrifugal quantum states is much smaller than the mirror radius and the effective centrifugal acceleration could be approximated as constant with high accuracy. On the other hand, the Fermi potential of a mirror cannot be considered as infinitely high—just the opposite: the quantum-state energy is close to the value of the Fermi potential. Therefore in contrast to the gravitationally bound quantum states, neutrons tunnel deeply into the mirror (compared to the characteristic size of the wave functions). This phenomenon has to be taken into account. Another essential difference is related to the effects of surface roughness: as far as the characteristic scale of the centrifugal quantum states is much smaller, the roughness effects are much larger; therefore constraints for the cylindrical mirror surface are even more severe than those for flat mirrors in gravitational experiments. We will show rigorously in the following sections that the centrifugal quantum states could be described in a very similar way as the gravitational quantum states, although they are formed by completely different physical potentials. The large difference in the characteristic scales of the quantum states in the two cases requires different approaches for their experimental observation and study.

III. FORMAL SOLUTION

Neutrons with given energy E, scattered by a curved mirror, obey the following Schrödinger equation in cylindrical coordinates:

$$\left[-\frac{\hbar^2}{2M}\left(\frac{\partial^2}{\partial\rho^2}+\frac{1}{\rho}\frac{\partial}{\partial\rho}\right)-\frac{\hbar^2}{2M\rho^2}\frac{\partial^2}{\partial\varphi^2}+U(\rho,\varphi)-E\right]\Psi(\rho,\varphi)=0. \tag{1}$$

Here M is the neutron mass, ρ is the radial distance, measured from the center of mirror curvature (see Fig. 1), φ is the angle, and $U(\rho,\varphi)$ is the mirror Fermi potential. We will use the following steplike dependence for the mirror Fermi potential:

$$U(\rho,\varphi)=U_0\Theta(\rho-R)[\Theta(\varphi)-\Theta(\varphi-\varphi_0)],$$

where R is the mirror curvature radius and the angle φ_0 is determined by the mirror length L_{mirr} and the mirror curvature radius R via

$$\varphi_0=\frac{L_{mirr}}{2\pi R}.$$

In Eq. (1) we omitted the trivial dependence on the z coordinate along the curved mirror axis. By standard substitution $\Psi(\rho,\varphi)=\Phi(\rho,\varphi)/\sqrt{\rho}$, Eq. (1) is transformed to the following form:

$$\left[-\frac{\hbar^2}{2M}\left(\frac{\partial^2}{\partial\rho^2}\right)-\frac{\hbar^2}{2M\rho^2}\left(\frac{\partial^2}{\partial\varphi^2}+\frac{1}{4}\right)+U(\rho,\varphi)-E\right]\Phi(\rho,\varphi)=0. \tag{2}$$

Now the problem is formulated as follows. The incoming neutron flux is known at the curved mirror entrance. We have to find the neutron flux at the exit of the mirror with the angle coordinate φ_0. The measured neutron current component, parallel to the mirror surface, is

$$J(\rho,\varphi)=\frac{i\hbar}{2M\rho}\left(\Psi(\rho,\varphi)\frac{\partial\Psi^*(\rho,\varphi)}{\partial\varphi}-\Psi^*(\rho,\varphi)\frac{\partial\Psi(\rho,\varphi)}{\partial\varphi}\right). \tag{3}$$

We start with the formal solution of Eq. (1) in the domain $0\leqslant\varphi\leqslant\varphi_0$. We express a solution of Eq. (1) as a series expansion in the complete set of basis functions $\chi_\mu(\rho)$ [55–58]:

$$\Phi(\rho,\varphi)=\sum_\mu \chi_\mu(\rho)[c_\mu\exp(i\mu\varphi)+d_\mu\exp(-i\mu\varphi)], \tag{4}$$

where c_μ and d_μ are the expansion coefficients. The basis functions $\chi_\mu(\rho)$ are solutions of the following eigenvalue problem:

$$\left[-\frac{\hbar^2}{2M}\left(\frac{\partial^2}{\partial\rho^2}\right)+U_0\Theta(\rho-R)-E\right]\chi_\mu(\rho)=-\frac{\hbar^2(\mu^2-1/4)}{2M\rho^2}\chi_\mu(\rho), \tag{5}$$

$$\chi_\mu(\rho\to 0)=0, \tag{6}$$

$$\chi_\mu(\rho\to\infty)=\sin(\sqrt{2ME}\rho+\delta_\mu). \tag{7}$$

Here $\hbar^2(1/4-\mu^2)/(2M)\equiv-\hbar^2\eta^2/(2M)$ is the eigenvalue and δ_μ is the scattering phase. μ plays the role of the angular momentum. Let us note that the energy E is a fixed parameter in Eq. (5), while μ is the angular momentum eigenvalue to be found.

For the above-mentioned eigenvalue problem (5)–(7), self-adjointness of the corresponding Hamiltonian of radial motion is required for completeness of the basis set χ_μ [59]. One can prove that this requirement and the boundary conditions (6) and (7) are equivalent to the following condition for the eigenstates *phases*:

$$\delta_{\mu'}-\delta_\mu=\pi k, \tag{8}$$

where k is integer. In this case, the functions χ_μ are orthogonal to each other with the weight of $1/\rho^2$ on the interval $[0,\infty)$.

Note that there is no uniqueness condition for the wave function as long as $\varphi_0<2\pi$. So far, μ is no longer an integer value in our problem.

For a given positive energy $E>0$, the values μ form a discrete spectrum of *real* values if $\eta^2\geqslant 0$ and a continuum spectrum of complex values if $\eta^2<0$.

The flux (3) through a band with radial coordinates (ρ_1,ρ_2) orthogonal to the mirror surface in the mentioned basis can be expressed as

$$F(\varphi) = \int_{\rho_1}^{\rho_2} J(\rho,\varphi)d\rho$$
$$= \frac{\hbar}{M}\,\mathrm{Re}\sum_{\mu,\mu'}\left(\int_{\rho_1}^{\rho_2}\frac{\chi^*_{\mu'}(\rho)\chi_{\mu}(\rho)}{\rho^2}d\rho\right)\mu'$$
$$\times\{c_\mu c^*_{\mu'}\exp[i(\mu-\mu')\varphi]-d_\mu d^*_{\mu'}\exp[-i(\mu-\mu')\varphi]\}. \quad (9)$$

In the following we will be interested in the flux $F(\varphi)$ evolution as a function of the angle φ, which indicates the neutron density along the curved mirror. The neutron density is "initially" (i.e., for $\varphi=0$) localized by the collimator near the surface of the mirror in the band (ρ_1,ρ_2). Due to "dephasing" of φ-dependent exponents in expression (9) the neutron density within the band (ρ_1,ρ_2) decays rapidly when φ increases. We will find the rate of such a decay in the following sections. In particular, we will show that such a rate is determined by the lifetime of the quasistationary states formed by the superposition of the centrifugal potential and the Fermi potential of the mirror.

IV. CENTRIFUGAL QUASISTATIONARY STATES

To study the neutron states localized near the mirror surface, we will expand expression for the centrifugal energy in Eq. (5) in the vicinity of $\rho=R$. We introduce the deviation from the mirror surface, $z=\rho-R$, and get the following equation in the first order of the small ratio z/R:

$$\left[-\frac{\hbar^2}{2M}\frac{\partial^2}{\partial z^2}+U_0\Theta(z)+\hbar^2\frac{\mu_n^2-1/4}{2MR^2}(1-2z/R)-E\right]\chi_n(z)=0. \quad (10)$$

We will be interested in those solutions with different angular momenta μ_n, which correspond to the states of neutron, moving parallel to the mirror surface. Such neutrons with given energy $E=Mv^2/2$ possess angular momentum μ_n close to the classical value $\mu_0=MvR/\hbar$. Let us mention that the value of μ_0 is extremely high, $\mu_0\sim 5\times 10^8$, if $v=1000$ m/s and $R=2.5$ cm (parameters which can be realized in the experimental setup). Introducing new variables $\Delta_n=\mu_0-\mu_n$, where $\Delta_n\ll\mu_0$ and $\varepsilon_n=\hbar^2\mu_0\Delta_n/(MR^2)$, and keeping leading terms in μ_0, we get the following equation:

$$\left[-\frac{\hbar^2}{2M}\frac{\partial^2}{\partial z^2}+U_0\Theta(z)-\frac{Mv^2}{R}z-\varepsilon_n\right]\chi_n(z)=0. \quad (11)$$

Let us mention that the eigenvalue ε_n plays the role of energy in the above equation only formally. In fact, it defines the angular momentum eigenvalue

$$\mu_n=\mu_0-\frac{\varepsilon_n MR^2}{\mu_0\hbar^2}, \quad (12)$$

while the neutron energy E is a fixed parameter in our problem. The value ε_n can be interpreted as the radial motion energy within the above used linear expansion of the centrifugal potential in the vicinity of the curved mirror radius R.

Equation (11) describes the neutron motion in a constant effective field $a=-v^2/R$ superposed with the mirror Fermi potential $U_0\Theta(z)$. The sketch of corresponding potential is shown in Fig. 2.

The regular solution of Eq. (11) is given by the well-known Airy function [60]

$$\chi_n(z)\sim\begin{cases}\mathrm{Ai}(z_0-z/l_0-\varepsilon_n/\varepsilon_0) & \text{if } z>0,\\ \mathrm{Ai}(-z/l_0-\varepsilon_n/\varepsilon_0) & \text{if } z\leqslant 0.\end{cases} \quad (13)$$

Here

$$l_0=[\hbar^2R/(2M^2v^2)]^{1/3} \quad (14)$$

is the characteristic distance scale of the problem and

$$\varepsilon_0=[\hbar^2Mv^4/(2R^2)]^{1/3} \quad (15)$$

is the characteristic energy scale, $z_0=U_0/\varepsilon_0$. For the typical experimental setup parameters $U_0=150$ neV, $v=1000$ m/s, and $R=2.5$ cm, the above-mentioned scales are $l_0=0.04$ μm, $\varepsilon_0=15.3$ neV, and $z_0\simeq 10$.

The above-mentioned effective potential supports existence of the quasistationary states. They correspond to the solution of Eq. (11) with the outgoing wave boundary condition

$$\tilde{\chi}_n(z)\sim\begin{cases}\mathrm{Bi}(z_0-z/l_0-\varepsilon_n/\varepsilon_0)+i\mathrm{Ai}(z_0-z/l_0-\varepsilon_n/\varepsilon_0) & \text{if } z>0,\\ \mathrm{Ai}(-z/l_0-\varepsilon_n/\varepsilon_0) & \text{if } z\leqslant 0.\end{cases} \quad (16)$$

The complex energies of such quasistationary states can be found from the matching of the logarithmic derivative at $z=0$:

$$\varepsilon_n\equiv\varepsilon_0\lambda_n, \quad (17)$$

$$\mathrm{Ai}'(-\lambda_n)[\mathrm{Bi}(z_0-\lambda_n)+i\mathrm{Ai}(z_0-\lambda_n)]$$
$$=\mathrm{Ai}(-\lambda_n)[\mathrm{Bi}'(z_0-\lambda_n)+i\mathrm{Ai}'(z_0-\lambda_n)]. \quad (18)$$

The real and imaginary parts of the eigenvalue λ, obtained by numerical solution of Eq. (18) for two lowest states, are shown as a function of dimensionless variable z_0 in Figs. 3 and 4.

One can get a semiclassical approximation for the widths of the centrifugal quasistationary states if $|\lambda_n|\gg 1$ and $z_0\gg|\lambda_n|$ [49]. In this case one can use the asymptotic expressions for the Airy functions of large argument to get the following equation:

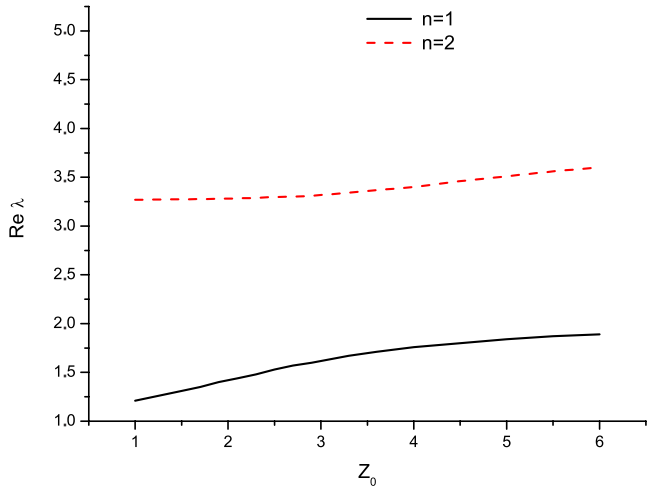

FIG. 3. (Color online) The real part of two lowest eigenvalues λ as a function of z_0 obtained by numerical integration of Eq. (18).

$$\sqrt{\frac{\lambda_n}{z_0-\lambda_n}}\tan\left(\frac{2}{3}\lambda_n^{3/2}-\pi/4\right)=1-2i\exp[-4/3(z_0-\lambda_n)^{3/2}]. \tag{19}$$

Also one can get a semiclassical approximation for the width Γ_n and λ_n from the above expression, valid for large n:

$$\lambda_n \simeq \left(\frac{3}{4}\pi(2n-1/2)\right)^{2/3} - \sqrt{\frac{\left[\frac{3}{4}\pi(2n-1/2)\right]^{2/3}}{z_0-\left[\frac{3}{4}\pi(2n-1/2)\right]^{2/3}}}, \tag{20}$$

$$\Gamma_n \simeq 4\varepsilon_0\frac{\sqrt{z_0-\lambda_n}}{z_0}\exp[-4/3(z_0-\lambda_n)^{3/2}]. \tag{21}$$

In the above expressions, $n=1,2,\ldots$. is an integer number. The angular momentum eigenvalue, corresponding to the

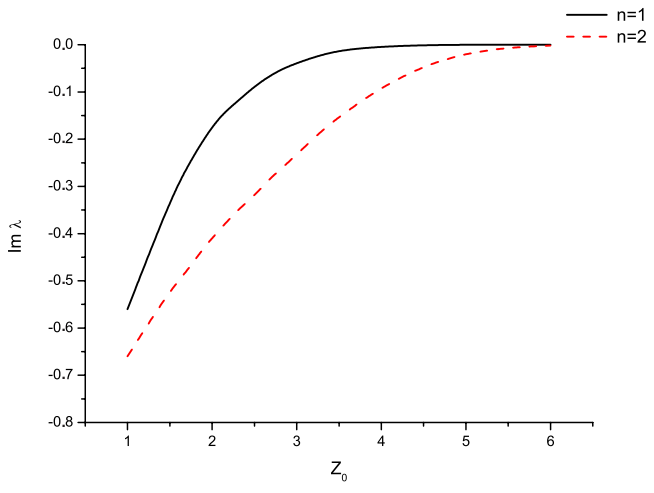

FIG. 4. (Color online) The imaginary part of the two lowest eigenvalues λ as a function of z_0 obtained by numerical integration of Eq. (18).

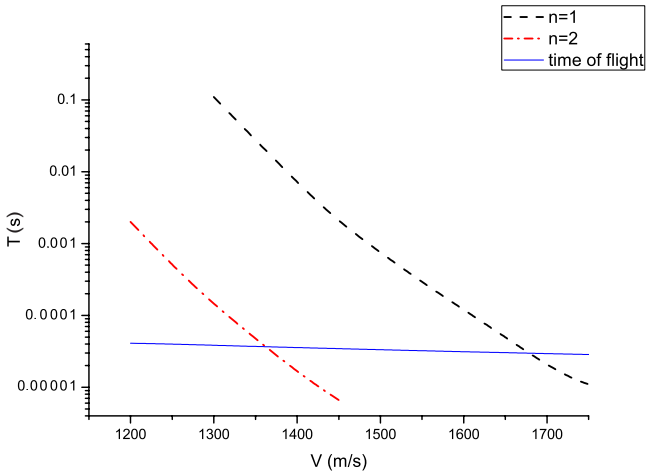

FIG. 5. (Color online) The lifetime of the two lowest neutron centrifugal quasistationary states is shown as a function of the neutron velocity. The mirror curvature radius equals $R=2.5$ cm, the mirror length is 5 cm, and the mirror Fermi potential is $U_0=150$ neV. The nearly horizontal solid line indicates the time of flight along the curved mirror.

complex energy ε_n of the quasistationary states, obtains a positive imaginary part, according to (12):

$$\text{Im}\,\mu_n=\frac{\Gamma_n R}{2\hbar v}. \tag{22}$$

The energy and the width of the quasistationary states depend strongly on the centrifugal acceleration $|a|=v^2/R$. A small acceleration a results in a broad barrier, which separates the states in the effective well from the continuum. Indeed, $z_0=U_0/\varepsilon_0=U_0[(2R^2)/(\hbar^2Mv^4)]^{1/3}$ increases if v decreases. The widths of the quasistationary states decrease exponentially as is seen from expression (21). Besides that, the effective well becomes broader and new quasi-stationary states appear with decreasing of a (in analogy with the appearance of new bound states with increasing the size of the well). Equation (19) enables us to estimate the critical values of the neutron velocity v_c, which corresponds to the appearance of new states in the effective well:

$$z_0=\lambda_n^0=[3/2\pi(n-3/4)]^{2/3}.$$

Taking into account that $z_0=U_0/\varepsilon_0$ we conclude that

$$v_c^n=\left[\frac{U_0^3}{[3/2\pi(n-3/4)]^2}\frac{2R^2}{\hbar^2M}\right]^{1/4}. \tag{23}$$

The accuracy of the above approximation increases with n.

The lifetime of the two lowest quasistationary quantum states as a function of the neutron velocity, obtained from solving Eq. (18) is shown in Fig. 5 for the mirror with the Fermi potential $U_0=150$ neV (sapphire) and in Fig. 6 for the mirror with the Fermi potential $U_0=54$ neV (silicium). The critical velocity values scale with the Fermi potential as $v_c\sim U_0^{3/4}$.

The above-mentioned quasistationary states play an essential role in neutron density evolution near the mirror surface as a function of φ. We will show that under certain

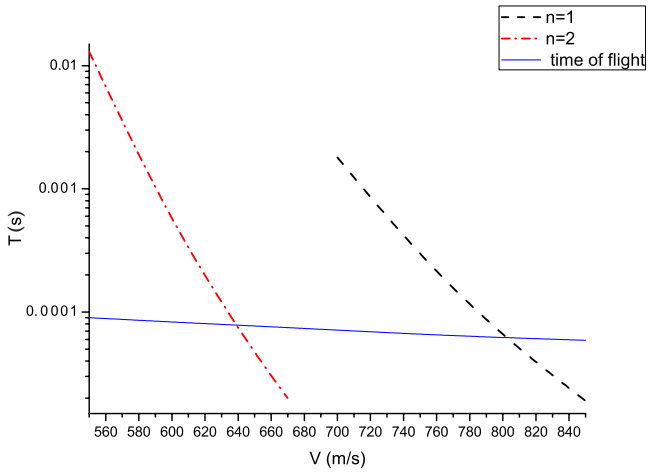

FIG. 6. (Color online) The lifetime of the two lowest neutron centrifugal quasistationary states is shown as a function of the neutron velocity. The mirror curvature radius equals $R=2.5$ cm, the mirror length is 5 cm, and the mirror Fermi potential is $U_0=54$ neV. The nearly horizontal solid line indicates the time of flight along the curved mirror.

conditions the expansion (9) can be substituted by a few effective terms, corresponding to the contribution of quasistationary states. To clarify the role of quasistationary states, it would be more convenient to use a time-dependent formalism.

V. TIME-DEPENDENT APPROACH

Let us return to the expansion (9) for the neutron current through the band of dimension $h=\rho_2-\rho_1 \ll R$, orthogonal to the mirror surface. Taking into account very large values of the angular momenta of the neutron "near-surface" states ($\mu \sim \mu_0 \simeq 5\times 10^8$), we can use the semiclassical character of motion along the φ variable. It is characterized by the contribution of fast oscillating exponents $\exp(i\mu\varphi)$. This enables us to treat φ as a classical variable. Namely, we will assume that neutrons follow a classical "trajectory" along φ:

$$\varphi = \omega t = \frac{vt}{R}.$$

The evolution along φ is then substituted by the evolution of the time-dependent wave function. Taking into account the relation between the angular momentum and the energy eigenvalues (12), we come to the following expression:

$$F(t) = \frac{v}{R}\,\mathrm{Re}\sum_{n,n'}\left(\int_{\rho_1}^{\rho_2}\chi_{n'}^{*}(\rho)\chi_n(\rho)d\rho\right) \times\{c_n c_{n'}^{*}\exp[i(\varepsilon_n'-\varepsilon_n)t/\hbar]\}, \tag{24}$$

with the functions $\chi_n(\rho)$ being solutions of (11). In the above expression we neglected backscattering and put coefficients $d_n=0$. Also we took into account the size of the band, $\rho_2-\rho_1=h\ll R$, where the neutron density is measured.

Thus we arrive at the problem of the time evolution (instead of the angular variable φ evolution) of an initially localized wave packet in the band with radial dimension $h=\rho_2-\rho_1$, which moves in the effective homogeneous field $a=v^2/R$. As was shown in [61] the integration over energies in (24) results in two terms. One term reflects the existence of S-matrix poles in the complex energy plane, which are situated close to the real axis and correspond to the complex energies of quasistationary states. So far, this term describes the decay of the quasistationary states and the characteristic time scale is given by the corresponding widths $\tau_n=\hbar/\Gamma_n$.

The second term reflects the nonresonant contribution of all other energies (which do not match with energies of the quasistationary states). The characteristic time $\tau_{cl}=\sqrt{2hR/v^2}$ for such neutrons is equal to the classical time of passage of distance h with constant acceleration v^2/R. This time of passage is much smaller than the time that the neutron spends in the quasistationary states $\tau_{cl}\ll\tau_n$.

For the times $\tau_{cl}\ll t\ll\tau_n$ the quasistationary-state contribution is dominant. This enables us to neglect the nonresonant contribution in the expansion (24) and to take into account only the quasistationary-state contribution:

$$F(t)\approx\frac{v}{R}\sum_{n'}|C_{n'}|^2\exp(-\Gamma_{n'}t). \tag{25}$$

Here n' indicates the quasistationary state number and $|C_{n'}|^2$ is the initial population of a given quasistationary state.

The sharp increase in the quasistationary-state lifetime (21) with decreasing the velocity below v_n (23), can be used for experimental observation of such states. Indeed, when the neutron velocity decreases the contribution of new quasistationary states increases rapidly. This results in the steplike dependence of the deflected neutron flux as a function of v. There are no quasistationary states for $v\gg v_c^1$, and therefore all neutrons traverse the mirror without being deflected. There are many quasistationary states in the opposite limit $v\ll v_c^1$, and therefore we deal with the classical reflection from the curved mirror. In Fig. 7 the flux of deflected neutrons is shown as a function of the neutron velocity. Under the assumptions made above the problem of deflection of cold neutrons ($v\sim 10^3$ m/s) by the curved mirror is analogous to the problem of the passage of ultracold neutrons through the slit between a horizontal mirror and an absorber in the presence of Earth's gravitational field, studied in detail in [45–52]. In the cited experiments the spatial density of neutrons in the gravitational states was scanned by changing the position of the absorber above the mirror. In the case of neutron motion along the curved mirror surface, the initial velocity variation results in changing the spatial dimension of the effective well, which bounds the neutron near the surface, ensuring the "scanning" of the quasistationary states.

The experimental observation of the centrifugal states of neutrons could be, however, complicated by the diffuse scattering of neutrons from the the mirror surface roughness. Below we will estimate the additional broadening of the centrifugal states due to the scattering on a rough surface.

VI. EFFECT OF ROUGHNESS

The effect of roughness consists in transferring the high neutron velocity parallel to the mirror surface into a velocity

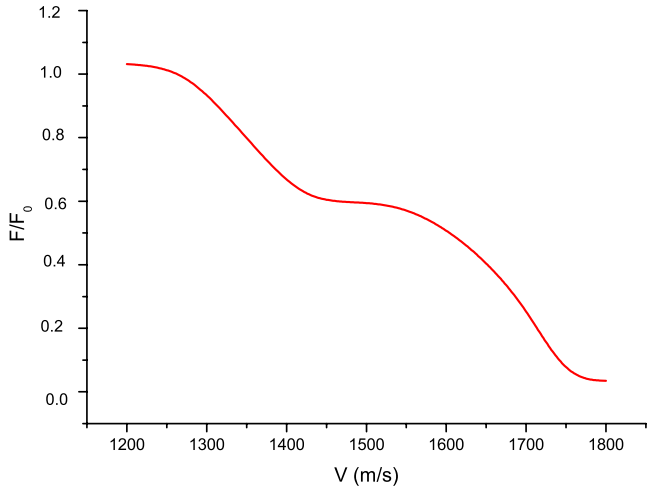

FIG. 7. (Color online) The relative flux of neutrons, deflected by the curved mirror, as a function of the neutron velocity. F_0 is the flux calculated at $v=1200$ m/s. The mirror curvature radius is $R=2.5$ cm, the mirror length is $L_{mirr}=5$ cm, and the mirror Fermi potential is $U_0=150$ neV.

component normal to the surface. As a result, the quasistationary centrifugal states acquire additional "ionization" width. The detailed theory of neutron rough-surface interactions can be found in [50,51]. To obtain a simple estimation of such a width we will follow the method developed in [49]. Namely, in the frame related to the neutron the mirror roughness appears as a time-dependent variation of the mirror position. We will start by treating a simple case of harmonic dependence:

$$U(z) = U_0\Theta(z + b_r \sin(\omega_r t)).$$

Here b_r is the roughness amplitude and ω_r is the roughness frequency, which can be related to the angular velocity of neutrons, ω, the mirror curvature radius R, and the characteristic length of roughness, l_r, via $\omega_r = \omega R/l_r$. Then the equation describing the evolution of initially localized wave packet gets the time-dependent right-hand side:

$$i\hbar\frac{d\Psi(z,t)}{dt} = \left[-\frac{\hbar^2}{2M}\frac{\partial^2}{\partial z^2} + U_0\Theta(z - b_r \sin(\omega_r t)) - \frac{Mv^2}{R}z\right]\Psi(z,t). \quad (26)$$

A solution of such an equation could be expanded in the set of eigenfunctions of the right-hand-side Hamiltonian, taken at instant t:

$$\left[-\frac{\hbar^2}{2M}\frac{\partial^2}{\partial z^2} + U_0\Theta(z - b_r \sin(\omega_r t)) - \frac{Mv^2}{R}z - \varepsilon_n(t)\right]u_n(z,t) = 0. \quad (27)$$

The corresponding expansion is

$$\Psi(z,t) = \sum_n C_n(t)u_n(z,t)\exp\left(-i\int_0^t \varepsilon(\tau)/\hbar d\tau\right). \quad (28)$$

Substitution of (28) into (26) yields in the coupled equation system for the time-dependent amplitudes $C_n(t)$

$$\frac{dC_n(t)}{dt} = -\sum_k \langle u_n|\frac{d}{dt}|u_k\rangle C_k(t)\exp[-i\omega_{nk}(t)]. \quad (29)$$

Here $\omega_{nk}(t) = \int_0^t [\varepsilon_k(\tau) - \varepsilon_n(\tau)]/\hbar d\tau$. It follows directly from (27) that

$$\langle u_n|\frac{d}{dt}|u_k\rangle = \frac{\langle u_n|\frac{dU}{dt}|u_k\rangle}{\varepsilon_n - \varepsilon_k}.$$

In the following we will consider the roughness small enough so that $U(z,t) \approx U_0\Theta(z) + U_0 b_r\omega_r \cos(\omega_r t)\delta(z)$. The coupling matrix elements are

$$\langle u_n|\frac{dU(z,t)}{dt}|u_k\rangle = b_r U_0\omega_r \cos(\omega_r t)u_n(0,t)u_k(0,t) \approx b_r U_0\omega_r \cos(\omega_r t)u_n(0,t=0)u_k(0,t=0).$$

Using an analog of the Fermi "golden rule," we get the following expression for ionization probability of centrifugal state n per unit of time:

$$P_{ion} = \frac{2\pi b_r^2 U_0^2 |u_n(0,t=0)u_f(0,t=0)|^2}{\hbar}\delta(\varepsilon_n + \hbar\omega_r - E_f)dk_f. \quad (30)$$

Here the index f labels the eigenstate of the final state of the continuum spectrum with energy E_f and wave number k_f. We assume that $E_f \gg \varepsilon_n$ for the neutron velocity $v \sim 10^3$ m/s and for realistic roughness parameters. This enables us to use the free-wave expression $u_f = 1/\sqrt{2\pi}\exp(ik_f z)$ for the final-state wave function. Taking into account the explicit form of u_n given by (16) and its semiclassical asymptotic, we get a simple estimation for P_{ion} of the nth quasistationary state:

$$P_{ion}^n \approx \frac{b_r^2 U_0^2}{\hbar^2 R l_0(z_0 - \lambda_n)\sqrt{2ME_f}}. \quad (31)$$

Taking into account the explicit expressions for the characteristic length, Eq. (14), and energy, Eq. (15), scales of the problem, we get for the case $z_0 \gg \lambda_n$

$$P_{ion} \approx \frac{b_r^2 U_0 v^2 M^2}{\hbar^2 R\sqrt{2ME_f}}. \quad (32)$$

To get the ionization width of the centrifugal state one should integrate the obtained probability with the spectral function of roughness $f(\omega)$, which provides the square of roughness amplitude as a function frequency:

$$\Gamma_i = \hbar\int_0^\infty \frac{b_r^2 f(\omega)U_0 v^2 M^2}{\hbar^2 R\sqrt{2M(\varepsilon_n + \hbar\omega)}}d\omega = \frac{\overline{b_r^2}U_0 v^2 M^2}{\hbar R\sqrt{2M\overline{E_f}}}. \quad (33)$$

Here $\overline{b_r^2}$ is the mean-square roughness and $\overline{E_f}$ is the mean ionization energy in the sense defined.

An important feature of the obtained result is the square dependence of ionization width on the neutron velocity and the roughness amplitude (for the case of small amplitudes,

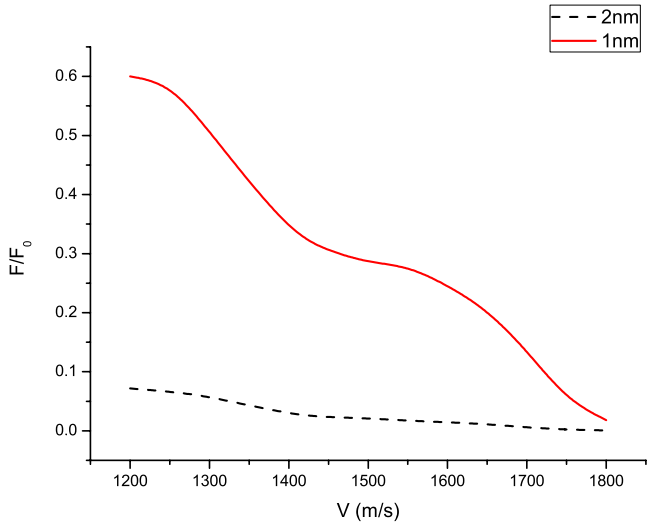

FIG. 8. (Color online) The relative flux of neutrons deflected by the curved sapphire mirror as a function of the neutron velocity. F_0 is the flux calculated at $v=1200$ m/s and zero roughness. The mirror curvature radius equals $R=2.5$ cm, the mirror length is $L_{mirr}=5$ cm, and the mirror Fermi potential is $U_0=150$ neV. The solid line corresponds to the roughness amplitude $b_r=1$ nm; the dashed line corresponds to roughness amplitude $b_r=2$ nm and roughness length $l_r=1$ μm.

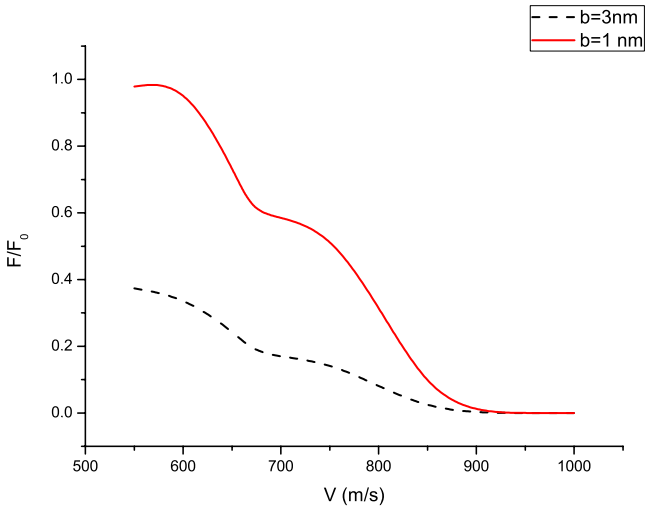

FIG. 9. (Color online) The relative flux of neutrons deflected by the curved silicon mirror as a function of the neutron velocity. F_0 is the flux calculated at $v=500$ m/s and zero roughness. The mirror curvature radius equals $R=2.5$ cm, the mirror length is $L_{mirr}=5$ cm, and the mirror Fermi potential is $U_0=54$ neV. The solid line corresponds to roughness amplitude $b_r=1$ nm; the dashed line corresponds to roughness amplitude $b_r=3$ nm and roughness length $l_r=1$ μm.

studied above). It constraints severely the roughness amplitudes acceptable for observation of the centrifugal states. In Fig. 8 we plot the neutron flux deflected by the curved sapphire mirror in the presence of roughness with amplitudes $b_r=1$ nm and $b_r=2$ nm. Figure 9 demonstrates the neutron flux deflected by the curved silicon mirror in the presence of roughness with amplitudes $b_r=1$ nm and $b_r=3$ nm. Thus the effect of roughness is reduced if the Fermi potential is low. Indeed, according to (23) and (33) we expect the following scaling law:

$$P_{ion} \sim U_0^{17/8}.$$

So the roughness amplitude of a sapphire mirror surface should be smaller than 1 nm (and 4 nm for a silicon mirror) to allow observation of the centrifugal states.

VII. CONCLUSIONS

We proposed a method for observation of the quasistationary states of neutrons, localized near a curved mirror surface. The effective bounding well is formed by a superposition of the centrifugal potential and the mirror Fermi potential. Reduction of the initial neutron velocity results in a spatial size increase of such a centrifugal trap, which, in its turn, results in the appearance of the quasistationary states in the spectrum of the system. This could be observed via a steplike dependence of the deflected neutron flux. We show that several centrifugal states can be observed, for instance, with a sapphire mirror (Fermi potential $U_0=150$ neV), with curvature radius $R=2.5$ cm, length $L_{mirr}\approx 5$ cm, and surface roughness amplitude <1 nm. The critical velocities corresponding to the steps in the deflected flux are $v_1=1700$ m/s and $v_2=1350$ m/s. The characteristic spatial dimension of the mentioned centrifugal states is $l_0\approx 0.04$ μm. In the case of a silicon mirror with the same shape (Fermi potential $U_0=54$ neV) the corresponding critical velocities values are $v_1=810$ m/s and $v_2=650$ m/s . Such neutron states could provide a promising tool for studying different types of neutron-matter interactions with the characteristic range of a few tens of nanometers.

ACKNOWLEDGMENTS

We are grateful to our colleagues from the GRANIT collaboration and participants of the GRANIT-2006 Workshop for stimulating discussions and ANR (Agence Nationale de la Recherche, France) for partial support of this work.

[1] J. W. Strutt Baron Rayleigh, *The Theory of Sound* (Macmillan, London 1878), Vol. 2.
[2] L. Rayleigh, Philos. Mag. **27**, 100 (1914).
[3] A. N. Oraevsky, Quantum Electron. **32**, 377 (2002).
[4] K. J. Vahala, Nature (London) **424**, 839 (2003).
[5] I. I. Goldman and V. D. Krivchenkov, *Problems in Quantum Mechanics* (Pergamon Press, London 1961).
[6] D. ter Haar, *Selected Problems in Quantum Mechanics* (Aca-

demic, New York, 1964).
[7] L. D. Landau and E. M. Lifshitz, *Quantum Mechanics: Non-relativistic Theory* (Pergamon, London, 1965).
[8] V. S. Flugge, *Practical Quantum Mechanics I* (Springer, Berlin, 1974).
[9] J. J. Sakurai, *Modern Quantum Mechanics* (Benjamin/Cummings, Menlo Park, 1985).
[10] P. W. Langhoff, Am. J. Phys. **39**, 954 (1971).
[11] J. Gea-Banacloche, Am. J. Phys. **67**, 776 (1999).
[12] V. V. Nesvizhevsky, H. G. Boerner, A. K. Petoukhov, H. Abele, S. Baeßler, F. J. Rueß, Th. Stoeferle, A. Westphal, A. M. Gagarski, G. A. Petrov, and A. V. Strelkov, Nature (London) **415**, 297 (2002).
[13] D. V. Ahluwalia, Mod. Phys. Lett. A **17**, 1135 (2002).
[14] M. Khorrami *et al.*, Ann. Phys. (N.Y.) **304**, 91 (2003).
[15] D. Bini, C. Cherubin, and B. Mashhoon, Phys. Rev. D **70**, 044020 (2004).
[16] C. Kiefer and C. Weber, Ann. Phys. (N.Y.) **14**, 253 (2005).
[17] M. Leclerc, Class. Quantum Grav. **22**, 3203 (2005).
[18] D. V. Ahluwalia-Khalilova, Int. J. Mod. Phys. D **14**, 2151 (2005).
[19] R. Banerjee, B. D. Roy, and S. Samanta, Phys. Rev. D **74**, 045015 (2006).
[20] F. Brau and F. Buisseret, Phys. Rev. D **74**, 036002 (2006).
[21] N. Boulanger, P. Spindel, and F. Buisseret, Phys. Rev. D **74**, 125014 (2006).
[22] F. Buisseret *et al.*, Class. Quantum Grav. **24**, 855 (2007).
[23] A. Accioly and H. Blas, Mod. Phys. Lett. A **22**, 961 (2007).
[24] A. Saha, Eur. Phys. J. C **51**, 199 (2007).
[25] R. B. Mann and M. B. Young, Class. Quantum Grav. **24**, 951 (2007).
[26] A. J. Silenko and O. V. Teryaev, Phys. Rev. D **76**, 061101(R) (2007).
[27] O. Bertolami and F. M. Nunes, Class. Quantum Grav. **20**, L61 (2003).
[28] V. V. Nesvizhevsky and K. V. Protasov, Class. Quantum Grav. **21**, 4557 (2004).
[29] V. V. Nesvizhevsky, G. Pignol, and K. V. Protasov, Phys. Rev. D **77**, 034020 (2008).
[30] S. Baeßler, V. V. Nesvizhevsky, K. V. Protasov, and A. Y. Voronin, Phys. Rev. D **75**, 075006 (2007).
[31] P. Watson, J. Phys. G **29**, 1451 (2003).
[32] R. Onofrio and L. Viola, Phys. Rev. A **53**, 3773 (1996).
[33] L. Viola and R. Onofrio, Phys. Rev. D **55**, 455 (1997).
[34] A. Herdegen and J. Wawrzycki, Phys. Rev. D **66**, 044007 (2002).
[35] J. Wawrzycki, Acta Phys. Pol. B **35**, 613 (2004).
[36] C. Chryssomalakos and D. Sudarsky, Gen. Relativ. Gravit. **35**, 605 (2003).
[37] G. Kalbermann, J. Phys. A **35**, 9829 (2002).
[38] R. W. Robinett, Phys. Rep. **392**, 1 (2004).
[39] M. Berberan-Santos, *et al.*, J. Math. Chem. **37**, 101 (2005).
[40] M. Belloni, *et al.*, Phys. Scr. **72**, 122 (2005).
[41] W. H. Mather and R. F. Fox, Phys. Rev. A **73**, 032109 (2006).
[42] D. Witthaut and H. J. Korsch, J. Phys. A **39**, 14687 (2006).
[43] E. Romera and F. de los Santos, Phys. Rev. Lett. **99**, 263601 (2007).
[44] G. Gonzalez, Rev. Mex. Fis. **54**, 5 (2008).
[45] V. V. Nesvizhevsky *et al.*, Nucl. Instrum. Methods Phys. Res. A **440**, 754 (2000).
[46] V. V. Nesvizhevsky *et al.*, J. Res. Natl. Inst. Stand. Technol. **110**, 263 (2005).
[47] V. V. Nesvizhevsky *et al.*, Phys. Rev. D **67**, 102002 (2003).
[48] V. V. Nesvizhevsky *et al.*, Eur. Phys. J. C **40**, 479 (2005).
[49] A. Y. Voronin, H. Abele, S. Baeszler, V. V. Nesvizhevsky, A. K. Petukhov, K. V. Protasov, and A. Westphal, Phys. Rev. D **73**, 044029 (2006).
[50] A. E. Meyerovich and V. V. Nesvizhevsky, Phys. Rev. A **73**, 063616 (2006).
[51] R. Adhikari, Y. Cheng, A. E. Meyerovich, and V. V. Nesvizhevsky, Phys. Rev. A **75**, 063613 (2007).
[52] A. Westphal *et al.*, Eur. Phys. J. C **51**, 367 (2007).
[53] V. I. Luschikov *et al.*, JETP Lett. **9**, 23 (1969).
[54] V. I. Luschikov and A. I. Frank, JETP Lett. **28**, 559 (1978).
[55] M. W. J. Bromley and B. D. Esry, Phys. Rev. A **68**, 043609 (2003).
[56] F. Sols and M. Macucci, Phys. Rev. B **41**, 11887 (1990).
[57] K. Lin and R. L. Jaffe, Phys. Rev. B **54**, 5750 (1996).
[58] O. Olendski and L. Mikhailovska, Phys. Rev. B **66**, 035331 (2002).
[59] A. M. Perelomov and V. S Popov, Theor. Math. Phys. **4**, 48 (1970).
[60] *Handbook of mathematical Functions*, edited by M. Abramowitz and I. E. Stegun (Dover, New York, 1965).
[61] A. I. Baz, Ya. B. Zeldovich, and A. M. Perelomov, *Scattering, Reactions and Decays in the Nonrelativistic Quantum Mechanics* (Israel Program for Scientific Translations, Jerusalem, 1969).